



Modeling and simulation of the infection zone from a cough

T. I. Zohdi¹

Received: 22 May 2020 / Accepted: 8 June 2020
© Springer-Verlag GmbH Germany, part of Springer Nature 2020

Abstract

The pandemic of 2020 has led to a huge interest of modeling and simulation of infectious diseases. One of the central questions is the potential infection zone produced by a cough. In this paper, mathematical models are developed to simulate the progressive time-evolution of the distribution of locations of particles produced by a cough. Analytical and numerical studies are undertaken. The models ascertain the range, distribution and settling time of the particles under the influence of gravity and drag from the surrounding air. Beyond qualitative trends that illustrate that large particles travel far and settle quickly, while small particles do not travel far and settle slowly, the models provide quantitative results for distances travelled and settling times, which are needed for constructing social distancing policies and workplace protocols.

Keywords Pandemic · Cough · Infection · Particles · Spread · Simulation

1 Introduction

The pandemic of 2020, due to SARS-CoV-2, named COVID-19 and referred to as coronavirus, has been responsible for hundreds of thousands of deaths in 2020 alone. It is well-established that this virus primarily spreads from person-to-person contact by respiratory droplets produced when an infected person coughs or sneezes. Subsequently, the droplets come into contact with the eyes, nose or mouth of a nearby person or when a person touches an infected surface, then makes contact with their eyes, nose or mouth. Since the virus is small, 0.06–0.14 microns in diameter, it can be contained in or attached to such emitted droplets. Droplets as small as one micron can carry enough viral load to cause an infection. A particular concern is the interaction of droplets with ventilation systems, which potentially could enhance the propagation of pathogens. This has implications on situation-specific safe distancing and the design of building filtration systems, air distribution, heating, air-conditioning and decontamination systems, for example using UV-c and related technologies. In order to facilitate such system redesigns, fundamental analysis tools are needed that are easy to use. Accordingly, this paper develops one type

of such needed tools, namely a simulator for the analysis of cough particle tracking, in order to ascertain how large is the potential infection zone and the airborne setting time of cough particles.

In its most basic form, a cough can be considered as a high-velocity release of a random distribution of particles of various sizes, into an ambient atmosphere. We refer the reader to Wei and Li [53], Duguid [11], Papineni and Rosenthal [37], Wei and Li [54], Zhu et al. [59], Chao et al. [9], Morawska et al. [31], VanSciver et al. [49], Kwon et al. [21], Tang et al. [46], Xie et al. [57], Gupta et al. [13], Wan et al. [52], Villafruela et al. [50], Nielson [33], Zhang and Li [58], Chao et al. [8] and Lindsley et al. [26] for extensive reviews of coughs and other respiratory emissions. Following formulations for physically similar problems associated with particulate dynamics from the fields of blasts, explosions and fire embers (Zohdi [64–67]), we make the following assumptions:

- We assume the same initial velocity magnitude for all particles under consideration, with a random distribution of outward directions away from the source of the cough. This implies that a particle non-interaction approximation is appropriate. Thus, the inter-particle collisions are negligible. This has been repeatedly verified by “brute-force” collision calculations using formulations found in Zohdi [60–63].
- We assume that the particles are spherical with a random distribution of radii R_i , $i = 1, 2, 3 \dots N = \text{particles}$.

✉ T. I. Zohdi
zohdi@me.berkeley.edu

¹ Department of Mechanical Engineering, University of California, 6195 Etcheverry Hall, Berkeley, CA 94720-1740, USA

The masses are given by $m_i = \rho_i \frac{4}{3} \pi R_i^3$, where ρ_i is the density of the particles.

- We assume that the cough particles are *quite small* and that the amount of rotation, if any, contributes negligibly to the overall trajectory of the particles. The equation of motion for the i th particle in the system is

$$m_i \dot{\mathbf{v}}_i = \Psi_i^{grav} + \Psi_i^{drag}, \quad (1.1)$$

with initial velocity $\mathbf{v}_i(0)$ and initial position $\mathbf{r}_i(0)$. The gravitational force is $\Psi_i^{grav} = m_i \mathbf{g}$, where $\mathbf{g} = (g_x, g_y, g_z) = (0, 0, -9.81) \text{ m/s}^2$.

- For the drag, we will employ a general phenomenological model

$$\Psi_i^{drag} = \frac{1}{2} \rho_a C_D ||\mathbf{v}^f - \mathbf{v}_i|| (\mathbf{v}^f - \mathbf{v}_i) A_i, \quad (1.2)$$

where C_D is the drag coefficient, A_i is the reference area, which for a sphere is $A_i = \pi R_i^2$, ρ_a is the density of the ambient fluid environment and \mathbf{v}^f is the velocity of the surrounding medium which, in the case of interest, is air. We will assume that the velocity of the surrounding fluid medium (\mathbf{v}^f) is given, implicitly assuming that the dynamics of the surrounding medium are unaffected by the particles.¹

In order to gain insight, initially, we will discuss the closely related, analytically tractable, Stokesian model next.

Remark As mentioned, there are a large number of physically similar phenomena to a cough, such as the particulate dynamics associated with blasts, explosions and fire embers. We refer the interested reader to the wide array of literature on this topic; see Plimpton [39], Martin-Alberca and Garcia-Ruiz [29], Brock [6], Russell [40], Shimanzu [43], Werrett [55], Kazuma [19,20], Wingerden et al. [56] and Fernandez-Pello [12], Pleasance and Hart [38], Stokes [45] and Rowntree and Stokes [42], Hadden et al. [14], Urban et al. [48] and Zohdi [67].

2 Analytical characterization: simplified Stokesian model

2.1 Analysis of particle velocities

For a (low Reynolds number) Stokesian model, the differential equation for each particle is (Fig. 1)

$$m_i \frac{d\mathbf{v}_i}{dt} = m_i \mathbf{g} + c_i (\mathbf{v}^f - \mathbf{v}_i)_i \quad (2.1)$$

¹ We will discuss these assumptions further, later in the paper.

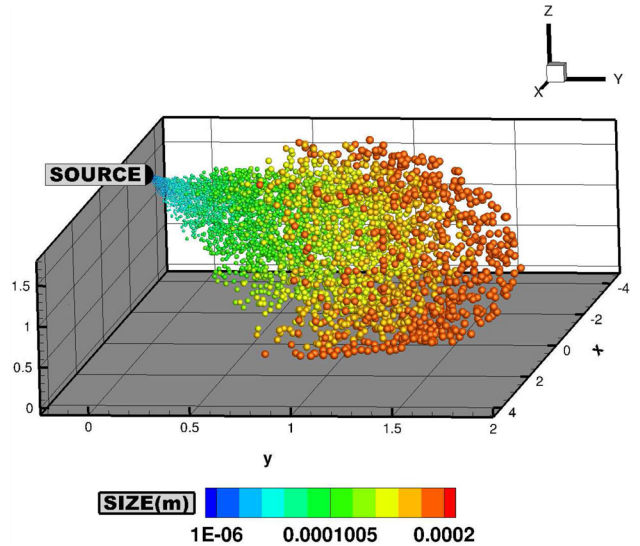


Fig. 1 Model problem for release of cough particles

where $c_i = \mu_f 6\pi R_i$, where μ_f is the viscosity of the surrounding fluid (air) and the local Reynolds number for a particle is $Re \stackrel{\text{def}}{=} \frac{2R_i \rho_a ||\mathbf{v}^f - \mathbf{v}_i||}{\mu_f}$ and μ_f is the fluid viscosity. This can be written in normalized form as

$$\frac{d\mathbf{v}_i}{dt} + \underbrace{\frac{c_i}{m_i} \mathbf{v}_i}_{a_i} = \underbrace{\mathbf{g} + \frac{c_i}{m_i} \mathbf{v}^f}_{b_i}. \quad (2.2)$$

This can be solved analytically to yield, for example in the z direction

$$v_{iz}(t) = \underbrace{(v_{izo} - \frac{b_{iz}}{a_{iz}})}_{A_{iz}} e^{-\frac{c_i}{m_i} t} + \underbrace{\frac{b_{iz}}{a_{iz}}}_{B_{iz}}, \quad (2.3)$$

where

- $a_{iz} = \frac{c_i}{m_i} = \frac{9\mu_f}{2\rho_i R_i^2}$,
- $b_{iz} = g_z + \frac{c_i}{m_i} = g_z + \frac{9\mu_f}{2\rho_i R_i^2}$,
- $A_{iz} = v_{izo} - (g_z \frac{2\rho_i R_i^2}{9\mu_f} + v_z^f)$,
- $B_{iz} = (g_z \frac{2\rho_i R_i^2}{9\mu_f} + v_{iz}^f)$,

where the same holds for the y and z directions. The trends are

- As $t \rightarrow \infty$

$$v_{iz}(t = \infty) \rightarrow \frac{2g_z \rho_i R_i^2}{9\mu_f} + v_z^f, \quad (2.4)$$

- As $R_i \rightarrow 0$

$$v_{iz}(t = \infty) \rightarrow v_z^f. \quad (2.5)$$

- The decay rate is controlled by $\frac{c_i}{m_i} = \frac{9\mu_f}{2\rho_i R_i^2}$, indicating that small particles attain ambient velocities extremely quickly.

Some special cases:

- With no gravity:

$$v_{iz}(t) = (v_{izo} - v_z^f)e^{-\frac{c_i}{m_i}t} + v_z^f. \quad (2.6)$$

- With no damping:

$$\frac{dv_{iz}}{dt} = g_z \Rightarrow v_{iz}(t) = v_{izo} + g_z t. \quad (2.7)$$

Again, we note that the equations are virtually the same for the x and y directions, with the direction of gravity and fluid flow being the main differentiators.

2.2 Analysis of particle positions

From the fundamental equation, relating the position \mathbf{r}_i to the velocity

$$\frac{d\mathbf{r}_i}{dt} = \mathbf{v}_i, \quad (2.8)$$

we can write for the z direction

$$\frac{dr_{iz}}{dt} = v_{iz} = A_{iz}e^{-\frac{c_i}{m_i}t} + B_{iz} \quad (2.9)$$

with the same being written for the x and y directions. Integrating and applying the initial conditions yields

$$r_{iz}(t) = r_{izo} + \frac{m_i}{c_i} A_{iz}(1 - e^{-\frac{c_i}{m_i}t}) + B_{iz}t. \quad (2.10)$$

If $g_z = 0$ and $v_z^f = 0$, then

$$r_{iz}(t) = r_{izo} + v_{izo}2\rho_i \frac{R_i^2}{9\mu_f}(1 - e^{-\frac{9\mu_f}{2\rho_i R_i^2}t}). \quad (2.11)$$

As $t \rightarrow \infty$

$$r_{iz}(\infty) = r_{izo} + v_{izo}2\rho_i \frac{R_i^2}{9\mu_f}. \quad (2.12)$$

As $R_i \rightarrow 0$, the travel distance is dramatically shorter. The converse is true, larger particles travel farther.

2.3 Settling (airborne) time

The settling, steady-state velocity can be obtained directly from

$$\frac{d\mathbf{v}_i}{dt} + a_i \mathbf{v}_i = \mathbf{b}_i, \quad (2.13)$$

by setting $\frac{d\mathbf{v}_i}{dt} = \mathbf{0}$, one can immediately solve for the steady-state velocity

$$\mathbf{v}_i(\infty) = \frac{\mathbf{b}_i}{a_i} = \frac{2\rho_i R_i^2}{9\mu_f} \mathbf{g} + \mathbf{v}^f. \quad (2.14)$$

The trends are

- As $R_i \rightarrow 0$, then $\mathbf{v}_i(\infty) \rightarrow \mathbf{v}^f$,
- As $\mathbf{v}_i^f \rightarrow \mathbf{0}$, then $\mathbf{v}_i(\infty) \rightarrow \frac{2\rho_i R_i^2}{9\mu_f} \mathbf{g}$.

In summary

- Large particles travel far and settle quickly and
- Small particles do not travel far and settle slowly.

Remark The ratio of the Stokesian drag force to gravity is

$$\frac{||\Psi^{drag, Stokesian}||}{||\Psi^{grav}||} = \frac{9\mu_f ||\mathbf{v}^f - \mathbf{v}_i||}{2\rho_i R_i^2 g}, \quad (2.15)$$

which indicates that for very small particles, drag will dominate the settling process and for larger particles, gravity will dominate.

3 Computational approaches for more complex models

3.1 More detailed characterization of the drag

In order to more accurately model the effects of drag, one can take into account that the empirical drag coefficient varies with Reynolds number. For example, consider the following piecewise relation (Chow [9]):

- For $0 < Re \leq 1$, $C_D = \frac{24}{Re}$,
- For $1 < Re \leq 400$, $C_D = \frac{24}{Re^{0.646}}$,
- For $400 < Re \leq 3 \times 10^5$, $C_D = 0.5$,
- For $3 \times 10^5 < Re \leq 2 \times 10^6$, $C_D = 0.000366 Re^{0.4275}$,
- For $2 \times 10^6 < Re < \infty$, $C_D = 0.18$,

where, as in the previous section, the local Reynolds number for a particle is $Re \stackrel{\text{def}}{=} \frac{2R_i \rho_a ||\mathbf{v}^f - \mathbf{v}_i||}{\mu_f}$ and μ_f is the fluid

viscosity.² We note that in the zero Reynolds number limit, the drag is Stokesian. In order to solve the governing equation,

$$\begin{aligned} m_i \dot{\mathbf{v}}_i &= \Psi_i^{grav} + \Psi_i^{drag} \\ &= m_i \mathbf{g} + \frac{1}{2} \rho_a C_D ||\mathbf{v}^f - \mathbf{v}_i|| (\mathbf{v}^f - \mathbf{v}_i) A_i, \end{aligned} \quad (3.1)$$

we integrate the velocity numerically

$$\begin{aligned} \mathbf{v}_i(t + \Delta t) &= \mathbf{v}_i(t) + \frac{1}{m_i} \int_t^{t+\Delta t} (\Psi_i^{grav} + \Psi_i^{drag}) dt \\ &\approx \mathbf{v}_i(t) + \frac{\Delta t}{m_i} (\Psi_i^{grav}(t) + \Psi_i^{drag}(t)). \end{aligned} \quad (3.2)$$

The position is obtained by integrating again:

$$\mathbf{r}_i(t + \Delta t) = \mathbf{r}_i(t) + \int_t^{t+\Delta t} \mathbf{v}_i(t) dt \approx \mathbf{r}_i(t) + \Delta t \mathbf{v}_i(t). \quad (3.3)$$

This approach has been used repeatedly for a variety of physically similar drift-type problems in Zohdi [64–67].

Remark The piecewise drag law of Chow [9] is a mathematical description for the Reynolds number over a wide range and is a curve-fit of extensive data from Schlichting [44].

3.2 Simulation parameters

In order to illustrate the model, the following simulation parameters were chosen:

- Starting height of 2 m,
- Total simulation duration, 4 s,
- The time step size, $\Delta t = 10^{-6}$ s,
- The cough velocity, $V^c(t = 0) = 30$ m/s (taken from the literature which indicates 10 m/s $\leq V^c \leq 50$ m/s),
- Density of particles, $\rho_i = 1000$ kg/m³,
- Density of air, $\rho_a = 1.225$, kg/m³ and
- Total mass, $M^{Total} = \sum_{i=1}^{P_n} m_i = 0.0005$ kg.

3.2.1 Particle generation

A mean particle radius was chosen to be $\bar{R} = 0.0001$ m with variations according to

$$R_i = \bar{R} \times (1 + A \times \zeta_i), \quad (3.4)$$

where $A = 0.9975$ and a random variable $-1 \leq \zeta_i \leq 1$. The algorithm used for particle generation was:

² The viscosity coefficient for air is $\mu_f = 0.000018$ Pa s.

- M=0
- Start loop: $i = 1, P_n$
- $R_i = \bar{R} \times (1 + A \times \zeta_i)$,
- $M = M + m_i = M + \rho_i \frac{4}{3}\pi R_i^3$
- If $M \geq M^{Total}$ then stop (determines P_n = particles)
- End loop

3.2.2 Initial trajectories

The initial trajectories we determined from the following algorithm

- Specify relative direction ‘cone’ parameters: $N^c = (N_x^c, N_y^c, N_z^c)$,
- For each particle, $i = 1, 2, 3, \dots, P_n$, construct a (perturbed) trajectory vector:

$$\begin{aligned} \mathbf{N}_i &= (N_x^c + A_x^c \times \eta_{ix}, N_y^c + A_y^c \times \eta_{iy}, N_z^c + A_z^c \times \eta_{iz}) \\ &= (N_{ix}, N_{iy}, N_{iz}), \end{aligned} \quad (3.5)$$

where $-1 \leq \eta_{ix} \leq 1, 0 \leq \eta_{iy} \leq 1$ and $-1 \leq \eta_{iz} \leq 1$.

- For each particle, normalize the trajectory vector:

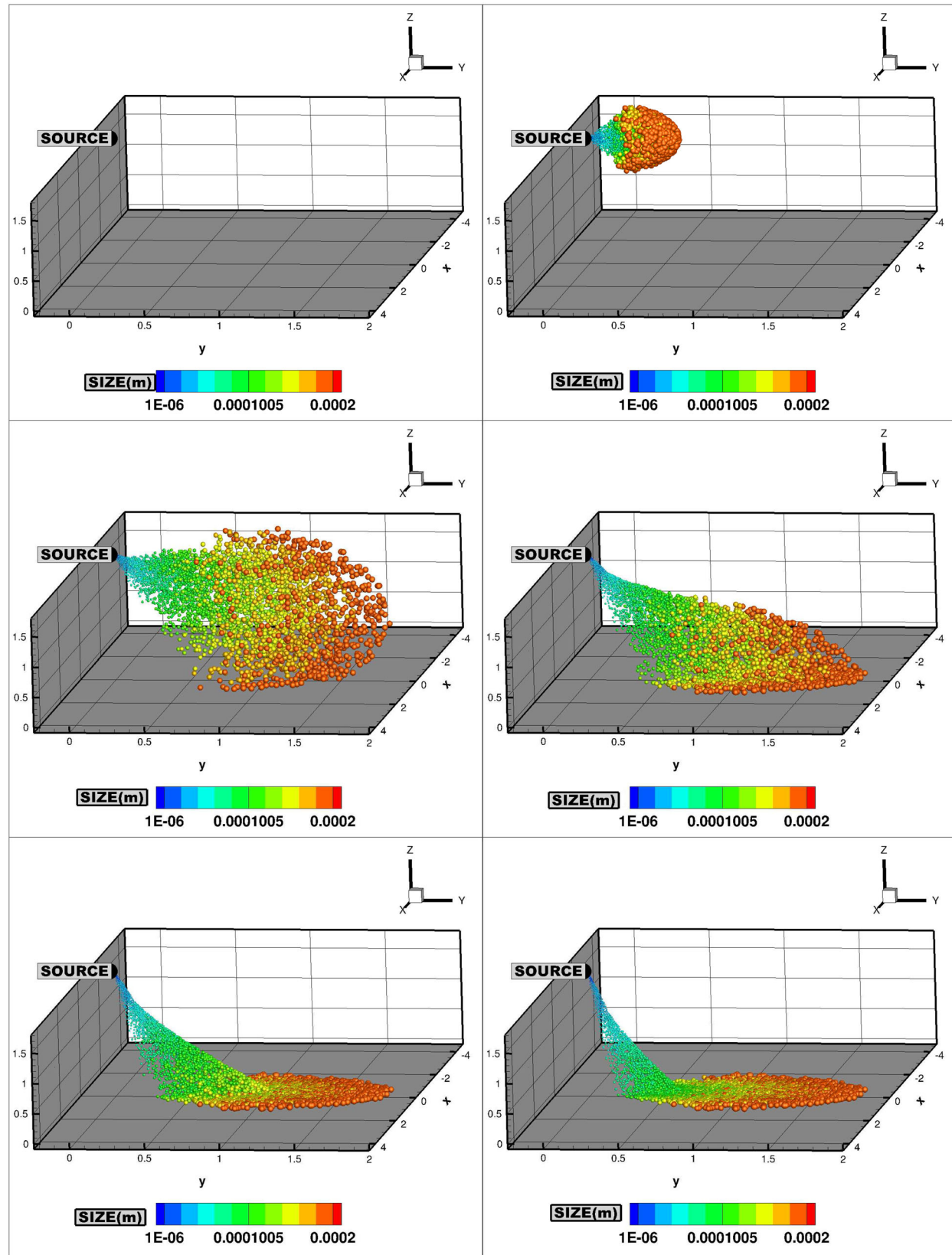
$$\mathbf{n}_i = \frac{1}{||\mathbf{N}_i||} (N_{ix}, N_{iy}, N_{iz}). \quad (3.6)$$

- For each particle, the velocity vector is constructed by a projection onto the normal vector:

$$\mathbf{v}_i = V^c \mathbf{n}_i. \quad (3.7)$$

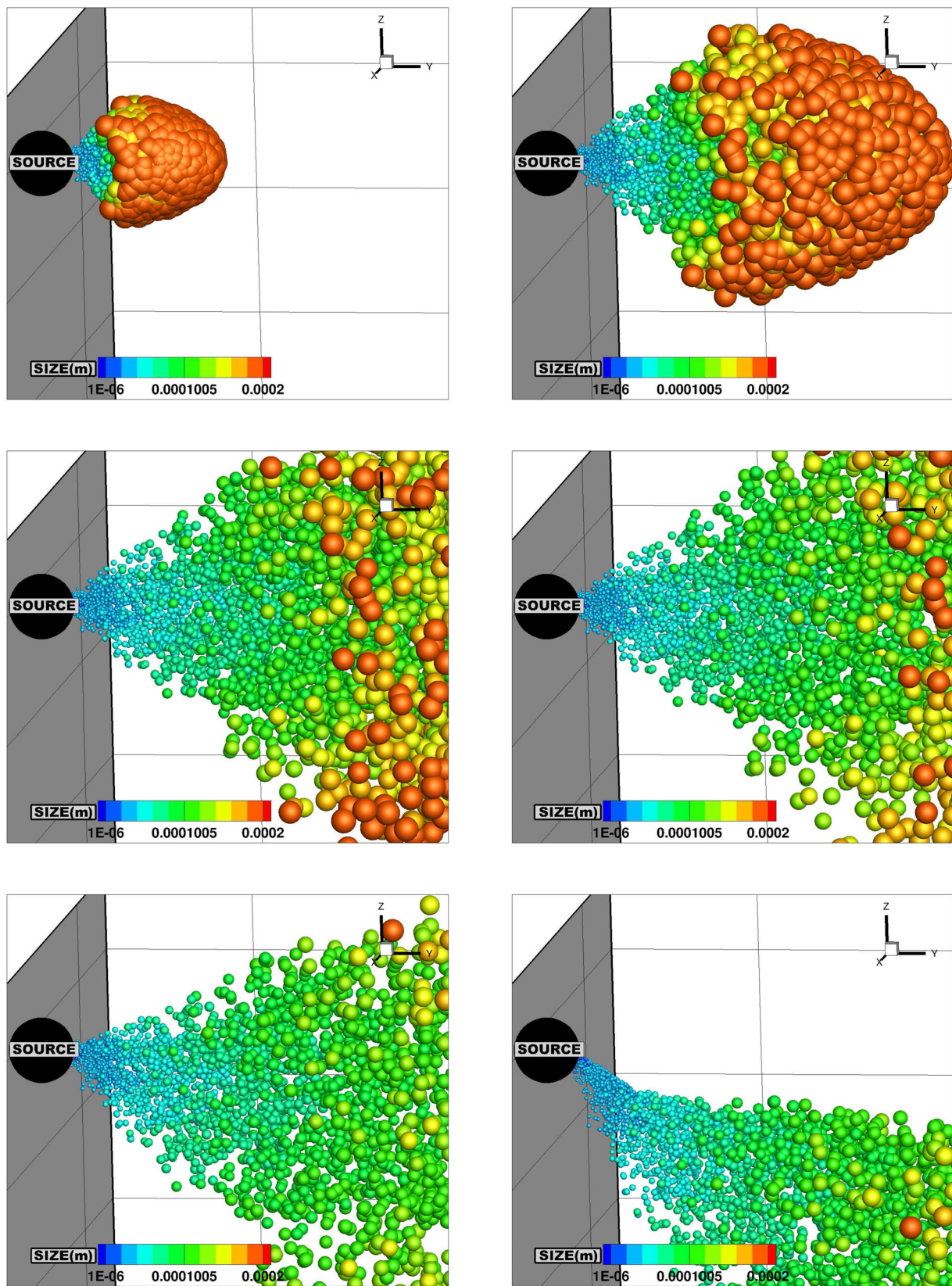
3.2.3 Numerical results

An extremely small (relative to the total simulation time) time-step size of $\Delta t = 10^{-6}$ s was used. Further reductions of the time-step size produced no noticeable changes in the results, thus the solutions generated can be considered to have negligible numerical error. The simulations took under 10 s on a standard laptop. The algorithm generated 59,941 particles ranging from 2.5×10^{-7} m $\leq R_i \leq 2 \times 10^{-4}$ m (i.e. 0.25 microns $\leq R_i \leq 200$ microns). We used a trajectory cone of $N^c = (0, 1, 0)$ and $A^c = (1, 0.5, 1)$ in the example given. Figures 2, 3 illustrate the results for the parameters above (for $v_y^f = 0$). If particles contacted the floor, they were immobilized. The maximum distance travelled from the source located at (0, 0, 2) was 2.72 m (achieved by large particles). Table 1 shows variation in the headwind. For strong tailwind, the larger particles land further away from the cough source. As the analytical theory asserts, successive frames indicate that: (a) Large particles travel far and settle quickly and (b) Small particles do not travel far and settle slowly (when there are no ambient velocities). As observed



Accepted for publication in Computational Mechanics

Fig. 2 Cough simulation (from a starting height of 2 m, for $v^f = (0, 0, 0)$): successive frames indicating the spread of particles. **a** Large particles travel far and settle quickly and **b** small particles do not travel far and settle slowly



Accepted for publication in Computational Mechanics

Fig. 3 Zoom on cough simulation (from a starting height of 2 m, for $v^f = (0, 0, 0)$): successive frames indicating the spread of particles. **a** Large particles travel far and settle quickly and **b** small particles do not travel far and settle slowly

Table 1 Maximum distance from the source at the end of T = 4 s

v_y^f (m/s)	Max-distance (m)	Comments
-2.0	8.002	Due to small particles moving backwards
-1.0	4.210	Due to small particles moving backwards
0.0	2.721	Due to large particles moving forwards
1.0	4.937	Due to large particles moving forwards
2.0	8.736	Due to large particles moving forwards

in the simulations, the settling of the small particles is still not achieved by the end of the simulation time (here 4 s). Accordingly, the simulations were also run for extremely long periods to ascertain that the “mist” of small particles remained airborne for several minutes (as predicted by the theory). For strong opposing headwind, small particles move backwards, and still remain airborne for extended periods of time. *This is by far the most dangerous case, since this will encounter other persons at the torso level.* We also note that ratio of the general drag to gravity indicates:

$$\frac{||\Psi^{drag,general}||}{||\Psi^{grav}||} = \frac{3C_D\rho_{ia}||\mathbf{v}^f - \mathbf{v}_i||^2}{\rho_i R_i g}, \quad (3.8)$$

which indicates that at high velocities, the dynamics are dominated by drag.

4 Summary and extensions

For general cough conditions, there can be cases where the change in the surrounding fluid’s behavior, due to the motion of the particles and cough, may be important. The result is a system of coupled equations between the particles and the fluid, requiring spatio-temporal discretization (high-fidelity Finite Elements or Finite Differences) of the classical equations governing the surrounding fluid mechanics (Navier Stokes)

$$\begin{aligned} \text{Balance of mass : } & \frac{\partial \rho}{\partial t} = -\nabla_x \rho \cdot \mathbf{v} - \rho \nabla_x \cdot \mathbf{v}, \\ \text{Balance of momentum : } & \rho \left(\frac{\partial \mathbf{v}}{\partial t} + (\nabla_x \mathbf{v}) \cdot \mathbf{v} \right) = \nabla_x \cdot \boldsymbol{\sigma} + \mathbf{f}, \\ \text{Constitutive Law : } & \boldsymbol{\sigma} = -P\mathbf{1} + \lambda \text{tr} \mathbf{D} \mathbf{1} + 2\mu \mathbf{D} \\ & = -P\mathbf{1} + 3\kappa \frac{\text{tr} \mathbf{D}}{3} \mathbf{1} + 2\mu \mathbf{D}', \end{aligned} \quad (4.1)$$

where $\rho(\mathbf{x})$ is the density field of the fluid, $\mathbf{v}(\mathbf{x})$ is the fluid velocity field, $\boldsymbol{\sigma}(\mathbf{x})$ is the fluid stress field, $\mathbf{D}(\mathbf{x})$ is the fluid velocity gradient field, $\mathbf{f}(\mathbf{x})$ is the body force field, $P(\mathbf{x})$ is the fluid pressure field, $\lambda(\mathbf{x})$ and $\mu(\mathbf{x})$ are fluid material

property fields.³ It is important to emphasize that physically compatible boundary data must be applied, and this is not a trivial matter for compressible flow. Additionally, the first law of thermodynamics should be included (along with equations for various chemical reactions), which reads as

$$\rho \dot{w} - \boldsymbol{\sigma} : \nabla_x \mathbf{v} + \nabla_x \cdot \mathbf{q} - \rho z = 0, \quad (4.2)$$

where $w(x)$ is the stored energy in the fluid, $\mathbf{q}(x)$ is the heat flux field, z is the heat source field per unit mass. Generally such models are ineffective for rapid real-time use, but are quite useful for detailed offline background analyses, where a rapid response is a nonissue. The continuum discretization is usually combined with a Discrete Element Method for the particle dynamics. There are a variety of such approaches, for example, see Avci and Wriggers [2], Onate et al. [34,35], Leonardi et al. [23], Onate et al. [36], Bolintineanu et al. [4] and Zohdi [60,63]. Such models are significantly more complex than the models used in the current paper. More detailed analyses of fluid-particle interaction can be achieved in a direct, brute-force, numerical schemes, treating the particles as part of the fluid continuum (as another fluid or solid phase), and thus meshing them in a detailed manner. In such an approach (for example see Avci and Wriggers [2])

- A fluid-only problem is solved, with (instantaneous) boundary conditions of $\mathbf{v}^f(\mathbf{x}) = \mathbf{v}_i(\mathbf{x})$ at each point on the fluid-particle boundaries, where the velocity of the points on the boundary are given by

$$\mathbf{v}_i(\mathbf{x}) = \mathbf{v}_i^{cm} + \boldsymbol{\omega}_i \times \mathbf{R}_{cm \rightarrow surf.}(\mathbf{x}), \quad (4.3)$$

where \mathbf{v}_i^{cm} is the center of mass and where $\boldsymbol{\omega}_i$ is the particle angular velocity for each of the individual particles and $\mathbf{R}_{cm \rightarrow surf.}$ is a vector from the mass center to the surface.

- For each particle, one would solve:

$$m_i \ddot{\mathbf{v}}_i = \Psi_i^{drag} + \text{other forces} \quad (4.4)$$

³ It is customary to specify \mathbf{v} and P on the boundary, and to determine ρ on the boundary through the Equation of State. P is given by an Equation of State.

and

$$I_i \dot{\omega}_i = \mathbf{M}_i^{drag} + \text{other moments} \quad (4.5)$$

where the forces and moments would have a contribution from the fluid drag (with particle occupying domain Ω_i and outward surface normal \mathbf{n}) is defined as

$$\Psi_i^{drag} = \int_{\partial\Omega_i} \boldsymbol{\sigma} \cdot \mathbf{n} dA, \quad (4.6)$$

and

$$\mathbf{M}_i^{drag} = \int_{\partial\Omega_i} \mathbf{R}_{cm \rightarrow surf.} \times \boldsymbol{\sigma} \cdot \mathbf{n} dA, \quad (4.7)$$

- At a time-step, the process is iteratively driven by solving the fluid-only problem first, then the particles-only problem, and repeated until convergence in an appropriate norm.

Along these lines, in Zohdi [60,63], more detailed, computationally intensive models were developed to characterize the motion of small-scale particles embedded in a flowing fluid where the dynamics of the particles affects the dynamics of the fluid and vice-versa. In such a framework, a fully implicit Finite-Difference discretization of the Navier-Stokes equations was used for the fluid and a direct particle-dynamics discretization is performed for the particles. Because of the large computational difficulty and expense of a conforming spatial discretization needed for large numbers of embedded particles, simplifying assumptions are made for the coupling, based on semi-analytical computation of drag-coefficients, which allows for the use of coarser meshes. Even after these simplifications, the particle-fluid system was strongly-coupled. The approach taken in that work was to construct a sub-model for each primary physical process. In order to resolve the coupling, a recursive staggering scheme was constructed, which was built on works found in Zohdi [60–63]. The procedure was as follows (at a given time increment): (1) each submodel equation (fluid or particle-system) is solved individually, “freezing” the other (coupled) fields in the system, allowing only the primary field to be active, (2) after the solution of each submodel, the associated field variable was updated, and the next submodel was solved and (3) the process is then repeated, until convergence. The time-steps were adjusted to control the rates of convergence, which is dictated by changes in the overall physics. Specifically, the approach was a staggered implicit time-stepping scheme, with an internal recursion that automatically adapted the time-step sizes to control the rates of convergence within a time-step. If the process did not converge (below an error tolerance) within a preset number of iterations, the time-step

was adapted (reduced) by utilizing an estimate of the spectral radius of the coupled system. The developed approach can be incorporated within any standard computational fluid mechanics code based on finite difference, finite element, finite volume or discrete/particle element discretization (see Labra and Onate [22], Onate et al. [34,35], Rojek et al. [41] and Avci and Wriggers [2]). However, while useful in many industrial applications where high precision is required, the use of such a model for the coarser applications of interest in this work is probably unwarranted.

In closing, we remark on a closely related theme to the one described in this paper, namely *decontamination*. For example, decontamination based on UV technology has become ubiquitous, with many variants now being proposed. UV light varies in wavelength from 10 to 400 nm, thus making it shorter than visible wavelengths and larger than x-rays. Short wave UV light (UV-c) can damage DNA and sterilize surfaces making it useful in the medical industry. This was first noted in 1878 (Downes and Blunt [10]) when the effect of short-wavelength light killing bacteria was discovered. By 1903 it was known the most effective wavelengths were around 250 nm (UV-c), for which Niels Finsen won a Nobel Prize (for skin-based tuberculosis eradication using UV light). Contaminants in the indoor environment are almost entirely organic carbon-based compounds, which break down when exposed to high-intensity UV at 240–280 nm. Despite the attractiveness of using UV-c light, the literature has shown that it is difficult to ensure that all surfaces are completely decontaminated due to shadowing effects. Thus, the use of ultraviolet germicidal irradiation (UVGI) is effective only as a component in a multistage process—it alone carries the risk of residual contamination. Thus, purely UV-c protocols should be adopted if there is no other choice. However, they can be an integral part of a multistage process involving a combination of (a) gas vapors and (b) heat and humidity. The topic of decontamination technologies is of paramount interest (see references Anderson et al. [1], Battelle [3], Boyce et al. [5], Card et al. [7], Heimbuch and Harish [15], Heimbuch et al. [16], Ito and Ito [17], Lin et al. [24], Kanemitsu [18], Lindsley et al. [25], Lore et al. [27], Marra et al. [28], Mills et al. [30], Tseng and Li [47], Viscusi et al. [51] and Nerandzic et al. [32]), and the corresponding simulation of such processes has recently been undertaken in Zohdi [68] and is a topic of ongoing research.

References

1. Anderson JG, Rowan NJ, MacGregor SJ, Fouracre RA, Farish O (2000) Inactivation of food-borne enteropathogenic bacteria and spoilage fungi using pulsed-light. IEEE Trans Plasma Sci 28(1):83–88

2. Avci B, Wriggers P (2012) A DEM-FEM coupling approach for the direct numerical simulation of 3D particulate flows. *J Appl Mech* 79:010901-1–7
3. Battelle (2020) Instructions for healthcare personnel: preparation of compatible N95 respirators for decontamination by the Battelle Memorial Institute using the Battelle Decontamination System. <https://www.fda.gov/media/137032/download>. Accessed May 2020
4. Bolintineanu DS, Grest GS, Lechman JB, Pierce F, Plimpton S, Schunk PR (2014) Particle dynamics modeling methods for colloid suspensions. *Comput Part Mech* 1(3):321–356
5. Boyce JM (2016) Modern technologies for improving cleaning and disinfection of environmental surfaces in hospitals. *Antimicrob Resist Infect Control* 5:10. <https://doi.org/10.1186/s13756-016-0111-x>
6. Brock ASH (1949) A history of fireworks. George G. Harrap and Co., London
7. Card KJ, Crozier D, Dhawan A, Dinh M, Dolson E, Farrokhan N, Gopalakrishnan V, Ho E, King ES, Krishnan N, Kuzmin G, Maltas J, Pelesko J, Scarborough JA, Scott JG, Sedor G, Weaver DT (2020) UV sterilization of personal protective equipment with idle laboratory biosafety cabinets during the Covid-19 pandemic. *Occup Environ Health*. <https://doi.org/10.1101/2020.03.25.20043489>
8. Chao CYH, Wan MP, Morawska L, Johnson GR, Ristovski ZD, Hargreaves M et al (2009) Characterization of expiration air jets and droplet size distributions immediately at the mouth opening. *J Aerosol Sci* 40(2):122–133
9. Chow CY (1980) An introduction to computational fluid dynamics. Wiley, New York
10. Downes A, Blunt TP (1878) On the influence of light upon protoplasm. *Proc R Soc Lond* 28(190–195):199–212. <https://doi.org/10.1098/rspa.1878.0109>
11. Duguid JP (1946) The size and the duration of air-carriage of expiratory droplets and droplet-nuclei. *J Hyg* 44:471–479
12. Fernandez-Pello AC (2017) Wildland fire spot ignition by sparks and firebrands. *Fire Saf J* 91:2–10
13. Gupta JK, Lin CH, Chen Q (2009) Flow dynamics and characterization of a cough. *Indoor Air* 19(6):517–525
14. Hadden R, Scott S, Lautenberger C, Fernandez-Pello CA (2011) Ignition of combustible fuel beds by hot particles: an experimental and theoretical study. *Fire Technol* 47:341–355
15. Heimbuch B, Harnish D (2019) Research to mitigate a shortage of respiratory protection devices during public health emergencies (report to the FDA No. HHSF223201400158C). Applied Research Associate, Inc
16. Heimbuch BK, Wallace WH, Kinney K, Lumley AE, Wu C-Y, Woo M-H, Wander JD (2011) A pandemic influenza preparedness study: use of energetic methods to decontaminate filtering facepiece respirators contaminated with H1N1 aerosols and droplets. *Am J Infect Control* 39(1):e1–e9
17. Ito A, Ito T (1986) Absorption spectra of deoxyribose, ribosephosphate, ATP and DNA by direct transmission measurements in the vacuum-UV (150–190 nm) and far-UV (190–260 nm) regions using synchrotron radiation as a light source. *Photochem Photobiol* 44(3):355–358
18. Kanemitsu K et al (2005) Does incineration turn infectious waste aseptic? *J Hosp Infect* 60(4):304–306
19. Kazuma S (2004) Hanabi no Hon. Fireworks Book, Tankosha. ISBN 4-473-03177-2
20. Kazuma S (2011) Wonder of fireworks. Soft Bank Creative, Tokyo
21. Kwon S-B, Park J, Jang J, Cho Y, Park D-S, Kim C et al (2012) Study on the initial velocity distribution of exhaled air from coughing and speaking. *Chemosphere* 87(11):1260–1264
22. Labra C, Onate E (2009) High-density sphere packing for discrete element method simulations. *Commun Numer Methods Eng* 25(7):837–849
23. Leonardi A, Wittel FK, Mendoza M, Herrmann HJ (2014) Coupled DEM-LBM method for the free-surface simulation of heterogeneous suspensions. *Comput Part Mech* 1(1):3–13
24. Lin T-H, Tang F-C, Hung P-C, Hua Z-C, Lai C-Y (2018) Relative survival of *Bacillus subtilis* spores loaded on filtering facepiece respirators after five decontamination methods. *Indoor Air* 28(5):754–762
25. Lindsley WG, Martin SB, Thewlis RE, Sarkisian K, Nwoko JO, Mead KR, Noti JD (2015) Effects of ultraviolet germicidal irradiation (UVGI) on N95 respirator filtration performance and structural integrity. *J Occup Environ Hyg* 12(8):509–517 10.1080/15459624.2015.1018518
26. Lindsley WG, Pearce TA, Hudnall JB, Davis KA, Davis SM, Fisher MA, Khakoo R, Palmer JE, Clark KE, Celik I, Coffey CC, Blachere FM, Beezhold DH (2012) Quantity and size distribution of cough-generated aerosol particles produced by influenza patients during and after illness. *J Occup Environ Hyg* 9(7):443–449. <https://doi.org/10.1080/15459624.2012.684582>
27. Lore MB, Heimbuch BK, Brown TL, Wander JD, Hinrichs SH (2011) Effectiveness of three decontamination treatments against influenza virus applied to filtering facepiece respirators. *Ann Occup Hyg* 56(1):92–101
28. Marra AR, Schweizer ML, Edmond MB (2018) No-touch disinfection methods to decrease multidrug-resistant organism infections: a systematic review and meta-analysis. *Infect Control Hosp Epidemiol* 39(1):20–31
29. Martin-Alberca C, Garcia-Ruiz C (2014) Analytical techniques for the analysis of consumer fireworks. *TrAC Trends Anal Chem* 35:27–36
30. Mills D, Harnish DA, Lawrence C, Sandoval-Powers M, Heimbuch BK (2018) Ultraviolet germicidal irradiation of influenza-contaminated N95 filtering facepiece respirators. *Am J Infect Control* 46(7):e49–e55
31. Morawska L, Johnson GR, Ristovski ZD, Hargreaves M, Mengersen K, Corbett S et al (2009) Size distribution and sites of origin of droplets expelled from the human respiratory tract during expiratory activities. *J Aerosol Sci* 40(3):256–269
32. Nerandzic MM, Cadnum JL, Pultz MJ, Donskey CJ (2010) Evaluation of an automated ultraviolet radiation device for decontamination of *Clostridium difficile* and other healthcare-associated pathogens in hospital rooms. *BMC Infect Dis* 10(1):197
33. Nielsen PV (2009) Control of airborne infectious diseases in ventilated spaces. *J R Soc Interface* 6(Suppl 6):S747–S755
34. Onate E, Idelsohn SR, Celigueta MA, Rossi R (2008) Advances in the particle finite element method for the analysis of fluid-multibody interaction and bed erosion in free surface flows. *Comput Methods Appl Mech Eng* 197(19–20):1777–1800
35. Onate E, Celigueta MA, Idelsohn SR, Salazar F, Suárez B (2011) Possibilities of the particle finite element method for fluid–soil–structure interaction problems. *Comput Mech* 48:307–318
36. Onate E, Celigueta MA, Latorre S, Casas G, Rossi R, Rojek J (2014) Lagrangian analysis of multiscale particulate flows with the particle finite element method. *Comput Part Mech* 1(1):85–102
37. Papineni RS, Rosenthal FS (1997) The size distribution of droplets in the exhaled breath of healthy human subjects. *J Aerosol Med* 10(2):105–116
38. Pleasance GE, Hart JA (1977) An examination of particles from conductors clashing as possible source of bushfire ignition. State Electricity Commission of Victoria (SEC), Victoria, Australia, Research and Development Department, report FM-1
39. Plimpton G (1984) Fireworks: a history and celebration. Doubleday, New York City
40. Russell MS (2008) The chemistry of fireworks. Royal Society of Chemistry, Great Britain. ISBN 978-0-85404-127-5
41. Rojek J, Labra C, Su O, Onate E (2012) Comparative study of different discrete element models and evaluation of equivalent

- micromechanical parameters. *Int J Solids Struct* 49:1497–1517. <https://doi.org/10.1016/j.ijsolstr.2012.02.032>
42. Rowntree G, Stokes A (1994) Fire ignition of aluminum particles of controlled size. *J Electr Electron Eng* 1994:117–123
 43. Shimizu T (1996) Fireworks: the art, science, and technique. Pyrotechnica Publications, Austin. ISBN 978-0-929388-05-2
 44. Schlichting H (1979) Boundary-layer theory, 7th edn. McGraw-Hill, New York
 45. Stokes AD (1990) Fire ignition by copper particles of controlled size. *J Electr Electron Eng Aust* 10:188–194
 46. Tang JW, Settles GS (2008) Coughing and aerosols. *N Eng J Med* 359(15):e19
 47. Tseng C-C, Li C-S (2007) Inactivation of viruses on surfaces by ultraviolet germicidal irradiation. *J Occup Environ Hyg* 4(6):400–405
 48. Urban JL, Zak CD, Song J, Fernandez-Pello AC (2017) Smolder spot ignition of natural fuels by a hot metal particle. *Proc Combust Inst* 36(2):3211–3218
 49. VanSciver M, Miller S, Hertzberg J (2011) Particle image velocimetry of human cough. *Aerosol Sci Technol* 45(3):415–422
 50. Villafruela JM, Olmedo I, Ruiz De Adana M, Mendez C, Nielsen PV (2013) CFD analysis of the human exhalation flow using different boundary conditions and ventilation strategies. *Build Environ* 62:191–200
 51. Viscusi DJ, Bergman MS, Eimer BC, Shaffer RE (2009) Evaluation of five decontamination methods for filtering facepiece respirators. *Ann Occup Hyg* 53(8):815–827
 52. Wan MP, Sze To GN, Chao CYH, Fang L, Melikov A (2009) Modeling the fate of expiratory aerosols and the associated infection risk in an aircraft cabin environment. *Aerosol Sci Technol* 43(4):322–343
 53. Wei J, Li Y (2016) Airborne spread of infectious agents in the indoor environment. *Am J Infect Control* 44(9):S102–S108
 54. Wei J, Li Y (2017) Human cough as a two-stage jet and its role in particle transport. *PLoS ONE*. <https://doi.org/10.1371/journal.pone.0169235>
 55. Werrett S (2010) Fireworks: pyrotechnic arts and sciences in European history. University of Chicago Press, Chicago
 56. Wingerden VK, Hesby I, Eckhoff R (2011) Ignition of dust layers by mechanical sparks. In: Proceedings of 7th global congress on process safety, Chicago, Ill, 2011
 57. Xie X, Li Y, Chwang ATY, Ho PL, Seto WH (2007) How far droplets can move in indoor environments-revisiting the Wells evaporation-falling curve. *Indoor Air* 17(3):211–225
 58. Zhang L, Li Y (2012) Dispersion of coughed droplets in a fully-occupied high-speed rail cabin. *Build Environ* 47:58–66
 59. Zhu S, Kato S, Yang J-H (2006) Study on transport characteristics of saliva droplets produced by coughing in a calm indoor environment. *Build Environ* 41(12):1691–1702
 60. Zohdi TI (2007) Computation of strongly coupled multifield interaction in particle-fluid systems. *Comput Methods Appl Mech Eng* 196:3927–3950
 61. Zohdi TI (2010) On the dynamics of charged electromagnetic particulate jets. *Arch Comput Methods Eng* 17(2):109–135
 62. Zohdi TI (2013) Numerical simulation of charged particulate cluster-droplet impact on electrified surfaces. *J Comput Phys* 233:509–526
 63. Zohdi TI (2014) Embedded electromagnetically sensitive particle motion in functionalized fluids. *Comput Part Mech* 1:27–45
 64. Zohdi TI (2016) A note on firework blasts and qualitative parameter dependency. *Proc R Soc*. <https://doi.org/10.1098/rspa.2015.0720>
 65. Zohdi TI, Cabalo J (2017) On the thermomechanics and footprint of fragmenting blasts. *Int J Eng Sci* 118:28–39
 66. Zohdi TI (2018) Modeling the spatio-thermal fire hazard distribution of incandescent material ejecta in manufacturing. *Comput Mech*. <https://doi.org/10.1007/s00466-018-1617-2>
 67. Zohdi TI (2020) A machine-learning framework for rapid adaptive digital-twin based fire-propagation simulation in complex environments. *Comput Methods Appl Mech Eng*. <https://doi.org/10.1016/j.cma.2020.112907>
 68. Zohdi TI (2020) Rapid simulation of viral decontamination efficacy with UV irradiation. *Comput Methods Appl Mech Eng*. <https://www.sciencedirect.com/science/article/pii/S0045782520304011>

Publisher's Note Springer Nature remains neutral with regard to jurisdictional claims in published maps and institutional affiliations.